Radionuclide Imaging in Ischemic Stroke

Wolf-Dieter Heiss

Max Planck Institute for Neurological Research, Cologne, Germany

Learning Objectives: On successful completion of this activity, participants should be able to describe (1) the physiologic and metabolic variables relevant for brain function and the radionuclides and methods to measure these variables in cerebrovascular disease, especially ischemic stroke; (2) the radionuclide methods to determine the thresholds of flow and metabolism relevant for preservation of function and morphology and the obtained values in their relevance to prognosis and potential treatment; and (3) the applications of radionuclide imaging for identifying pathophysiologic changes responsible for extension of ischemic lesions, for defining the hemodynamic reserve in vascular disease, for detecting remote effects outside the primary lesions, and for locating compensatory activation in disturbed functional networks.

Financial Disclosure: Dr. Heiss is supported by the Wolf-Dieter Heiss Foundation within the Max Planck Society. The author of this article has indicated no other relevant relationships that could be perceived as a real or apparent conflict of interest.

CME Credit: SNMMI is accredited by the Accreditation Council for Continuing Medical Education (ACCME) to sponsor continuing education for physicians. SNMMI designates each *JNM* continuing education article for a maximum of 2.0 AMA PRA Category 1 Credits. Physicians should claim only credit commensurate with the extent of their participation in the activity. For CE credit, SAM, and other credit types, participants can access this activity through the SNMMI website (http://www.snmmilearningcenter.org) through November 2017.

Ischemic stroke is caused by interruption or significant impairment of blood supply to the brain, which leads to a cascade of metabolic and molecular alterations resulting in functional disturbance and morphologic damage. The changes in regional cerebral blood flow and regional metabolism can be assessed by radionuclide imaging, especially SPECT and PET. SPECT and PET have broadened our understanding of flow and metabolic thresholds critical for maintenance of brain function and morphology: PET was essential in the transfer of the concept of the penumbra to clinical stroke and thereby had a great impact on developing treatment strategies. Receptor ligands can be applied as early markers of irreversible neuronal damage and can predict the size of the final infarcts, which is important for decisions on invasive therapy in large ("malignant") infarction. With SPECT and PET, the reserve capacity of the blood supply can be tested in obstructive arteriosclerosis, which is essential for planning interventions. The effect of a stroke on surrounding and contralateral primarily unaffected tissue can be investigated, helping to understand symptoms caused by disturbance in functional networks. Activation studies are useful to demonstrate alternative pathways to compensate for lesions and to test the effect of rehabilitative therapy. Radioisotope studies help to detect neuroinflammation and its effect on extension of tissue damage. Despite the limitations of broad clinical application of radionuclide imaging, this technology has a great impact on research in cerebrovascular diseases and still has various applications in the management of stroke.

Key Words: SPECT; PET; stroke; cerebral ischemia; penumbra; infarction; reperfusion; hemodynamic reserve; neuroinflammation; diaschisis; functional activation

J Nucl Med 2014; 55:1831–1841
DOI: 10.2967/jnumed.114.145003

Received Aug. 4, 2014; revision accepted Sep. 5, 2014.

For correspondence or reprints contact: Wolf-Dieter Heiss, Max Planck Institute for Neurological Research, Gleueler Strasse 50, 50931 Cologne, Germany.
E-mail: wdh@nf.mpg.de

Published online Oct. 9, 2014.

Cerebrovascular disease primarily affects the blood supply to the brain, which is high for providing the oxygen and glucose demand required for neuronal function of nervous tissue. Therefore, the measurement of cerebral blood flow (CBF) was and is a central task in research. Kety and Schmidt (*1*) introduced the first quantitative method to measure CBF using inhalation of inert gas—nitrous oxide—and following the rate of tissue uptake by analysis of multiple arterial and venous blood samples. This method quantified uptake of the tracer as the difference between arterial input and venous outflow and provided values of average blood flow per 100 g of tissue in the brain. With the injection of a radioactive inert gas into an artery supplying the brain, the accumulation and washout of the tracer from small regions of the cortex can be followed by external radiation detectors and the regional CBF (rCBF) can be determined by analysis of the clearance curve (*2*). ^{85}Kr—with its low-energy β radiation requiring measurement on the surgically exposed cortex—was soon replaced by ^{133}Xe, a γ-emitting radioactive gas with an energy permitting recording of the clearance curves through the intact skull (*3*). In the following years, the xenon method (intracarotid or intravenous injection of xenon in saline solution or inhalation of xenon gas) became the standard procedure to measure rCBF, and cerebral perfusion was quantitatively monitored in spatially discrete regions of the brain by use of multiple detectors (*4*) or a scintillation camera (*5*) providing 2-dimensional flow maps in healthy volunteers and patients with various brain disorders, including cerebrovascular disease (*6*). The advance of emission CT permitted 3-dimensional brain imaging of various physiologic parameters in addition to flow using either single-photon counting systems (SPECT) (*7*) or annihilation coincidence detection of positron-emitting radiopharmaceuticals (PET) (*8*). These emission CT techniques are now standard in nuclear medicine, and their applications in stroke are summarized in this review.

PHYSIOLOGIC VARIABLES AFFECTED IN ISCHEMIC STROKE

The energy demand of the nervous tissue is high, and therefore sufficient blood supply to the brain must be maintained consistently. The brain of a healthy man, containing approximately 130

billion neurons (21.5 billion in the neocortex) (*9*), comprises only 2% of total body mass yet at rest accounts for approximately 20% of the body's total basal oxygen consumption supplied by 15% of the cardiac blood output. The brain's oxygen consumption is almost entirely for the oxidative metabolism of glucose, which under normal physiologic conditions is the almost exclusive substrate for the brain's energy metabolism (*10*). Glucose metabolized in neuronal cell bodies is mainly to support cellular vegetative and housekeeping functions. Increases in glucose consumption (and regional blood flow) evoked by functional activation are confined to synapse-rich regions: overall, 59% of the total energy consumed is required by synaptic processes, 21% is required by action potential propagation, and only 20% is expended in maintaining membrane resting potential (*11*).

Cerebral blood volume (CBV) has at least 3 components, namely the arterial vessels, the capillaries, and the veins. The arterial fraction of the CBV in humans has been estimated to be about 30%; the venous-plus-capillary fraction of CBV is 63%–70%. Nondiffusible tracers used for measurement of CBV cannot obtain reliable values of tissue perfusion but assess the turnover rate of the regional blood pool. The average CBF of the normal whole brain is approximately 50 mL/100 g/min; blood flow to the gray matter is higher, at 80 mL/100 g/min; whereas flow to the white matter averages 20 mL/100 g/min. The brain receives about 15% of the cardiac output. Cerebral metabolic rate for oxygen ($CMRO_2$) averages about 3.2 mL/100 g/min, with the gray matter consuming approximately 6 mL/100 g/min and white matter consuming about 2 mL/100 g/min. Consequently, the normal arteriovenous oxygen content difference is about 6.4 vol%, corresponding to a jugular bulb oxygen saturation of between 65% and 70% in an individual with a normal hemoglobin concentration. Glucose is the main energy substrate used by the brain, and glucose consumed by the brain accounts for 25% of total-body glucose consumption at rest. In healthy volunteers, a mean glucose consumption of 29–32 μmol/100 g/min was found by means of ^{18}F-FDG PET (*12*), which corresponds well to whole-brain metabolic rates provided by the Kety–Schmidt method (*1*). The functional anatomy of the brain is reflected by the metabolic activity of individual regions. The highest values are found in the visual cortex (45–50 μmol/100 g/min) and in the striatum (42–46 μmol/100 g/min). Values are lower in other areas of the cerebral cortex and in the basal ganglia (35–42 μmol/100 g/min) and gray structures of the posterior cranial fossa (25–30 μmol/100 g/min). The lowest regional cerebral metabolic rate of glucose (rCMRGlc) is found in the white matter (15–22 μmol/100 g/min) (*13*). Up to 92% of the adenosine triphosphate in the brain comes from oxidative metabolism of glucose, supplying 12 mmol of adenosine triphosphate/100 g/min. The brain reserve of adenosine triphosphate and creatine phosphate totals only about 8 mmol, less than a minute's reserve. In the absence of oxygen, the anaerobic glycolysis of glucose and glycogen could supply only another 15 mmol of adenosine triphosphate. Loss of consciousness occurs when brain-tissue partial pressure of oxygen falls to 15–20 mm Hg. This level is reached in less than 10 s when CBF is completely stopped.

To maintain a sufficient supply of blood, oxygen, and glucose to the nervous tissue, the cerebral circulation is tightly regulated by several homeostatic mechanisms: flow–metabolism coupling (coupling to functional demand of tissue), CO_2 vasoreactivity (partial pressure of CO_2), partial pressure of oxygen (hypoxemia-induced cerebral vasodilation), and autoregulation (blood pressure and cerebral perfusion pressure).

RADIOACTIVE TRACERS USED IN STROKE

Radiopharmaceuticals for SPECT are usually limited to the assessment of CBV, hemodynamics, and cerebral perfusion. Nondiffusible tracers such as ^{131}I-labeled serum albumin were used to detect changes in vascular transit times due to circulatory disturbances, but information on tissue perfusion could not be obtained. For that purpose, radiotracers are required that cross the blood–brain barrier, distribute proportionally to rCBF, and remain fixed in the brain for a sufficient time to permit SPECT imaging. For tracers with a slow clearance from the brain, estimates of CBF are based on the microsphere model, but although the clinically used radiotracers do not satisfy all the requirements (free diffusibility, complete extraction from blood, fixation within the brain without redistribution), they follow rCBF closely enough to be clinically useful (*14*): ^{123}I-isopropyl iodoamphetamine is commercially distributed; peak activity is reached after 15–20 min, and with an injection dose of 111–222 MBq photon flux is low and image quality limited. ^{99m}Tc agents benefit from the optimal physical characteristics of the radionuclide (140-keV photon, 6-h half-life). Generators permit on-site labeling of the radiopharmaceuticals ^{99m}Tc-hexamethylpropyleneamine oxime (HMPAO) and ^{99m}Tc-ethyl cysteinate dimer (ECD); both tracers have rapid brain uptake but moderate first-pass extraction causing some underestimation of rCBF. ^{99m}Tc-HMPAO remains trapped in the brain, but blood clearance is slow and therefore perfusion deficits may be obscured. For ^{99m}Tc-ECD, brain uptake is rapid and clearance from the tissue is slow; because of rapid blood clearance, the brain-to-background activity ratio is higher than for ^{99m}Tc-HMPAO and image quality improved (*15,16*). Additionally, ^{99m}Tc-HMPAO is unstable in vitro and must be injected immediately after preparation, whereas ^{99m}Tc-ECD is stable and can be stored. Alternatively, CBF can be measured quantitatively after inhalation of ^{133}Xe gas, but the rapid clearance of the tracer requires specially designed instrumentation with high sensitivity in order to obtain multiple images during clearance of the low-energy tracer (81 keV) (*17*).

Radiotracers for PET emit a positron, which annihilates with an electron, resulting in emission of two 511-keV γ rays in opposite directions, which are used for coincidence counting. As isotopes, ^{11}C, ^{15}O, and ^{18}F are mainly used, and various compounds are labeled for imaging physiologic and metabolic variables.

Plasma tracers and red blood cell tracers have been proposed for measuring CBV, but for plasma tracers—^{68}Ga-ethylenediaminetetraacetic acid and ^{11}C-methylalbumin—problems with leakage of the blood–brain barrier and with reaching an equilibrium limit their application. Red blood cell tracers—carbon monoxide labeled with ^{11}C or ^{15}O—have been used extensively for measurement of CBV, and the values found in healthy subjects and in patients are in agreement with all other known methods (*18*). ^{11}C-labeled carbon monoxide may be used either by bolus inhalation or as a rapid succession of 2 or 3 normal inhalations. ^{15}O-labeled carbon monoxide has been used with single or brief inhalations (*19*) or has been given as a continuous inhalation (steady-state ^{15}O model).

The currently used methods to measure CBF with PET are based on the principles of inert freely diffusible tracers as in vivo autoradiography (*20*) with ^{15}O-H_2O as the flow tracer. These methods consist of a bolus administration of ^{15}O-H_2O or ^{15}O-CO_2 and a single 40-s PET scan measuring the tissue tracer concentration. The steady-state ^{15}O method uses either CO_2 or water labeled with ^{15}O by continuous administration. During the scan, ^{15}O activity in arterial blood is recorded and local CBF values are

calculated assuming a constant blood–brain equilibrium partition coefficient for the tracer.

Three different methods have been developed for the measurement of $CMRO_2$ using PET. The oldest is the ^{15}O continuous inhalation method (*21*), which involves the combined use of ^{15}O-labeled CO_2 and O_2. This method entails first the measurement of CBF with ^{15}O-CO_2 inhalation followed by measurement of the oxygen extraction ratio with $^{15}O_2$ inhalation imaging, corrected for recirculating labeled water by the ^{15}O-CO_2 scan. In addition, for accurate results, a correction for nonextracted intravascular ^{15}O is needed using a CBV scan. The second method involves the combined use of ^{15}O-labeled water and molecular oxygen to measure CBV, CBF, and oxygen extraction ratio (*22*). In this method, inhalation of molecular oxygen is used to estimate the oxygen extraction ratio pixel by pixel by means of an operational equation that explicitly requires the actual values for CBF and CBV in the same pixel. The CBV is usually measured by a single inhalation of ^{15}O-labeled carbon monoxide and CBF by the autoradiographic labeled water bolus method. This method is rapid (about 40 min in total is sufficient), and it is less sensitive to the problem of tissue heterogeneity than the steady-state method. The third method is the dynamic approach, in which dynamic PET scans are collected after inhalation of molecular oxygen as single or multiple breaths or by continuous inhalation. This permits simultaneous measurement of CBV, CBF, and $CMRO_2$ and volume of distribution of water from a single study (*23*).

The study of glucose metabolism with ^{18}F-FDG is a direct application of the autoradiographic technique (*24*) with ^{14}C-deoxyglucose. This model can be applied directly because the ^{18}F-FDG is transported into the cell in the same way as glucose and, with the aid of hexokinase, is phosphorylated to ^{18}F-deoxyglucose-6-phosphate. Deoxyglucose-6-phosphate, however, cannot be converted to fructose-6-phosphate and further degraded to CO_2 and H_2O but accumulates in the cell. The kinetics of the accumulation of deoxyglucose-6-phosphate can be described with the transport and enzyme constants of a 3-compartment model (*12*) for calculating the rCMRGlc.

A few other tracers—^{11}C-flumazenil, ^{123}I-iomazenil, ^{11}C-*N*-butan-2-yl-1-(2-chlorophenyl)-*N*-methylisoquinoline-3-carboxamide (PK11195), ^{18}F-misonidazol—have special research-oriented applications.

APPLICATIONS OF RADIOISOTOPE STUDIES IN STROKE

SPECT studies in cerebrovascular disease are confined mainly to the imaging of perfusion and rCBF and have confirmed and extended the results obtained with 2-dimensional CBF studies by the xenon technique. The rCBF patterns resulting from disturbances of regional blood supply due to large- or small-vessel disease or to emboli causing transient ischemic attacks or stroke described by 2-dimensional imaging (*25,26*) were extended in the third dimension and could be coregistered to morphologic images from CT or MR imaging. SPECT is widely available and can assess perfusion in brain tissue, but with the tracers that are usually applied (^{123}I-isopropyl iodoamphetamine, ^{99m}Tc-HMPAO, ^{99m}Tc-ECD), rCBF values are less reliable than those obtained by PET. Xenon SPECT permits quantitative measurements of rCBF without arterial blood sampling and is well suited for repeated studies within a short time, but the technique is still restricted to only a few centers and therefore only a few studies were performed in cerebrovascular disease. Only PET permits quantitative measurement of the physiologic variables relevant for maintaining function of nervous tissue and for the development of reversible and irreversible tissue damage, but multimodal PET measurements are restricted to a few centers and usually require arterial blood sampling. However, despite these limitations, PET studies made possible the transfer of experimental concepts into clinical studies and thereby improved the understanding of the pathophysiology of stroke, which is the basis for efficient treatment strategies.

Detection of the Ischemic Lesion

The localization and extent of lesions as a result of defects in blood supply can be assessed by SPECT studies of perfusion and by PET studies of flow or metabolism. Both techniques are more sensitive than CT for detecting both the presence and the extent of infarction (*27,28*). In the first 8 h after stroke, SPECT was shown to be positive in 90%, and sensitivities of 61%–74% and specificities of 88%–98% were reported (*29*). Early PET studies already showed discrepancies between flow and glucose uptake in ischemic areas, suggesting anaerobic glycolysis (*30*), and with determination of oxygen extraction ratio permitted researchers to follow the development of infarction within 48 h after the ictus (*31*). Increased perfusion was observed during this period despite irreversible tissue damage, which was termed luxury perfusion (*32*); in later stages, relative hyperemia can be observed in the core of infarcts as well as in the surrounding area (Fig. 1). Transient ischemic attacks can be differentiated from ischemic strokes within 6 h of symptom onset by, in SPECT, counting rate densities of 70% compared with the contralateral side (perfusion in stroke tissue 35%–60% of contralateral values) (*33*) and, in PET, significantly decreased CBF but increased oxygen extraction fraction (OEF) in affected regions (*34*).

SPECT findings have been shown to correlate with the severity of neurologic deficits and clinical outcome: early severe hypoperfusion

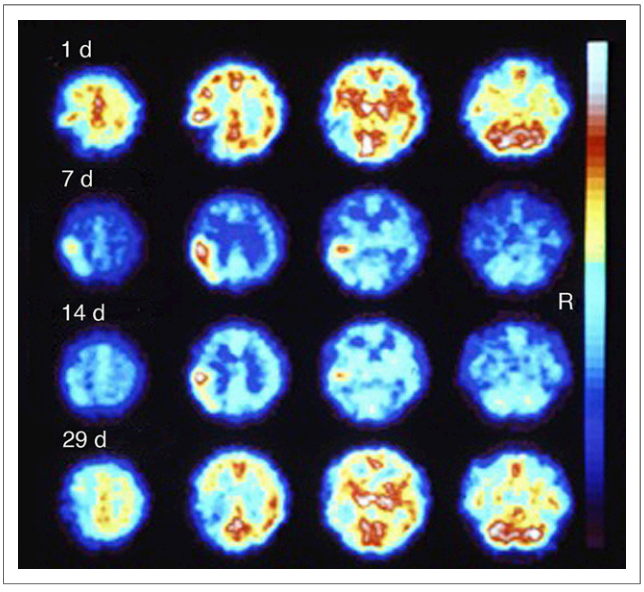

FIGURE 1. Four SPECT studies of ^{99m}Tc-HMPAO distribution in 47-y-old man. First study was approximately 20 h after right-sided hemiplegia and sensory aphasia had occurred. Profound decrease in uptake is seen in left parietal and temporal region. This area is surrounded in central and frontal directions by slightly increased tracer deposition. Seven and 14 d later, high uptake is seen in previously low-perfusion region. Last control study 29 d after insult shows decreased uptake in left parietal and temporal lobe and in left central and laterofrontal regions. Clinically, hemiplegia improved to hemiparesis and speech was still disturbed but improved. Late CT scan showed hypodense lesion in left parietal lobe.

predicted poor outcome better than neurologic deficit scores, especially when the volume of perfusion deficit was considered, and correlated to infarct size on late CT scans (*35*). Overall, SPECT had a significant added predictive value to neurologic scores, although it was not as reliable as PET, by which a classification of patients according to patterns of perfusion and oxygen consumption changes within 5–8 h of stroke onset predicted good or poor outcome and indicated critical states of ischemia amenable to therapy (*36*).

Identification of the Ischemic Penumbra

Pathophysiologic changes leading to functional impairment and irreversible tissue damage are the target for treatment of acute ischemic stroke (*37*). Experimental work on the ischemic flow thresholds of brain tissue demonstrated the existence of 2 critical levels of decreased perfusion: first, a level representing the flow threshold for reversible functional failure (functional threshold); second, a lower threshold below which irreversible membrane failure and morphologic damage occur. The range of perfusion values between those limits was called the ischemic penumbra (*38*), which was characterized by the potential for functional recovery without morphologic damage, provided that sufficient local blood flow could be reestablished. Whereas neuronal function is impaired immediately when blood flow drops below the threshold, the development of irreversible morphologic damage is time-dependent. This interaction of severity and duration of ischemia in the development of irreversible cell damage was established in simultaneous recordings of cortical neuronal activity and local blood flow (*39*). These results complement the concept of the ischemic penumbra: the potential for postischemic recovery of functionally impaired cells is determined not only by the level of residual flow in the ischemic phase but also by the duration of the flow disturbance.

Early PET studies on stroke have identified various tissue compartments within a brain territory compromised by ischemia (*40–43*). Tissue with rCBF lower than 12 mL/100 g/min or regional $CMRO_2$ lower than 65 μmol/100 g/min at the time of measurement (usually several hours after stroke) was found to be infarcted on late CT scans. Relatively preserved $CMRO_2$ was an indicator of maintained neuronal integrity in regions with CBF reduced to 12–22 mL/100 g/min. This pattern, coined misery perfusion (*41*), served as a definition of the penumbra that is characterized as the area of an increased OEF (up to >80% from the normal value of ~40%). PET studies allow the classification of 3 regions within the disturbed vascular territory: the core of ischemia (<12 mL/100 g/min), usually showing a transition into necrosis; a penumbral region (12–22 mL/100 g/min) of still viable tissue but with uncertain chances for infarction or recovery; and a hypoperfused area (>22 mL/100 g/min) not primarily damaged by the lack of blood supply (Fig. 2). The extent of the penumbra and its conversion into infarction is a dynamic process, and irreversible damage spreads from the core of ischemia to its border. This can be followed directly with advanced PET equipment, by which changes in the physiologic variables were studied in animal models and patients with acute stroke (Fig. 2) (*44–46*).

Experimental studies and clinical investigations at different time points after the attack (*47*) imply that the extent of the penumbra, that is, of morphologically intact but functionally impaired tissue, depends on the time of measurement relative to the onset of ischemia. Flow measurements in the first hours after a stroke permitted the identification of various compartments of tissue and their contribution to the final infarct on CT or MR imaging. If the threshold for probable infarction was set to the conventional value of 12 mL/100 g/min, and that for the upper limit of the penumbra was set to 18 mL/100 g/min, a large compartment of the final infarct (70%) was perfused below 12 mL/100 g/min; that is, at the level predicting necrosis, a smaller portion (18%) had flow values in the penumbral range (12–18 mL/100 g/min) and a fairly small compartment (12%) had perfusion at a higher level. Only the tissue with CBF above 12 mL/100 g/min could benefit from thrombolysis.

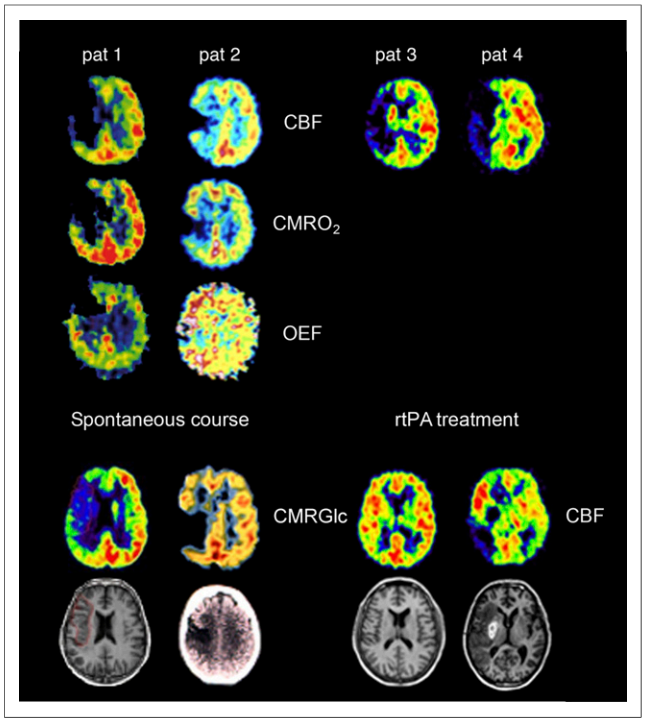

FIGURE 2. PET images of CBF, $CMRO_2$, and OEF in patients with acute ischemic stroke. (Left 2 columns) Areas with preserved OEF are not infarcted and can survive in spontaneous course (posterior part of ischemic cortex in patient 1, anterior part in patient 2 as indicated on CMRGlc and on late MR imaging and CT). (Right 2 columns) In patients receiving rtPA treatment, measurements of $CMRO_2$ and OEF are not feasible, but flow determinations show effect. If reperfusion occurs early enough and before tissue damage, tissue can be salvaged (patient 3). If reperfusion is achieved too late, tissue cannot be salvaged despite hyperperfusion in some parts (patient 4).

Assessment of critically perfused but viable tissue, which is amenable to reperfusion therapy, is difficult with SPECT perfusion studies because an indicator of tissue metabolism is not provided. Viability of some tissue compartments was indicated by reperfusion to brain regions with a ^{99m}Tc-HMPAO tissue uptake ratio to cerebellum of between 0.55 and 0.75 (*48*). Discriminant uptake ratios of ^{99m}Tc-ECD changed in the first hours after stroke from 45% to 52%, indicating that these values may be useful for therapeutic triage (*49*). Quantification of ^{99m}Tc-ECD SPECT values by Patlak plots permitted differentiation of the core of ischemia (<20 mL/100 g/min) and surrounding areas (20–52 mL/100 g/min) (*50*). In ^{99m}Tc-HMPAO SPECT studies, areas with residual CBF above 35 mL/100 g/min had a low possibility of infarction, regions with residual CBF above 25 mL/100 g/min could be recovered by early recanalization, but tissue with residual CBF below 20 mL/100 g/min was irreversibly damaged (*51*). These findings suggest that SPECT perfusion studies give results comparable to PET and support the utility of SPECT for selection of patients for treatment.

Noninvasive Imaging of the Penumbra

Measurement of blood flow values and determination of OEF by ^{15}O PET require arterial blood sampling. A marker of neuronal integrity is needed that does not require arterial blood sampling and can identify irreversibly damaged tissue irrespective of the time elapsed since the vascular attack. The central benzodiazepine receptor ligand ^{11}C-flumazenil binds to the γ-aminobutyric acid receptor abundant in the cerebral cortex. These receptors are sensitive to ischemic damage and can therefore identify early neuronal loss. With this tracer (Fig. 3), the pathophysiologic changes early after ischemic stroke could be accurately specified: 55% of the volume of the final infarct had ^{11}C-flumazenil uptake indicative of infarction in the first hours after stroke; 21% of the final infarct had flow below 14 mL/100 g/min but ^{11}C-flumazenil uptake above the critical value, thereby indicating penumbral tissue (*44*). Selective neuronal loss can also occur in tissue outside the documented penumbra or in reperfused penumbral areas, which can be documented by decreased cortical ^{11}C-flumazenil binding (*52*). With a comparable SPECT tracer, ^{123}I-iomazenil, irreversible tissue damage can be visualized in subacute or chronic stages of ischemic stroke (*53*). ^{123}I-iomazenil binding in ischemic brain tissue has been shown to correlate with $CMRO_2$ and OEF determined by PET (*54*), and ^{123}I-iomazenil uptake is preserved in brain regions with misery perfusion. ^{123}I-iomazenil SPECT has been shown to indicate neuronal loss in MR-defined mismatch areas (*55*); it can be used to identify patients who have a good or moderate prognosis for recovery from neurologic deficit after stroke.

MR studies using diffusion and perfusion imaging may provide a means of differentiation between the core and the penumbra: the early diffusion-weighted imaging (DWI) lesion may define the ischemic core, and adjacent critically hypoperfused tissue may be identified with perfusion-weighted imaging (PWI). Therefore, brain regions with hypoperfusion assessed by PWI but without restricted diffusion (PWI–DWI mismatch) were assumed to represent the penumbra (*56*): studies to validate mismatch as a surrogate for the penumbra demonstrated that the DWI lesion predicts more or less the finally infarcted tissue but that PWI data acquisition is inaccurate and the parameters used to estimate perfusion are variable and somewhat arbitrary. As a consequence, perfusion lesion size differs markedly and usually is overestimated. Time to peak delays of 4 and 6 s reliably identified hypoperfused and excluded normoperfused tissue but overestimated the volume of critically perfused but salvageable tissue (*57*): the mismatch volume in PWI–DWI as conventionally calculated therefore does not reliably reflect misery perfusion, that is, the penumbra as defined by PET (Fig. 4). Validation studies of PWI parameters on flow values obtained from $H_2{}^{15}O$ PET (*58*) resulted in corrections permitting reliable classification of critical, but potentially reversible, ischemia by time to maximum concentration, CBF, and time to peak concentration.

Markers of hypoxic tissue may be able to identify penumbral tissue. After promising animal experiments with nitroimidazole derivates, misonidazole, labeled with ^{18}F-fluoromisonidazole, was used (*59*) to image cerebral ischemia in humans and revealed increased uptake surrounding a zone of absent activity in 3 of 6 patients. This zone of high activity had disappeared when imaging was performed during the chronic phase, indicating that the hypoxic tissue had either infarcted or recovered. This pattern and time course was confirmed in a larger study (*60*). ^{18}F-fluoromisonidazole trapping detected 6.25–42.5 h after stroke onset was distributed over the periphery of the infarct and extended into normal tissue. The amount of hypoxic tissue detected by ^{18}F-fluoromisonidazole declined as a function of time after stroke onset. Volume of initially affected tissue and initial severity of neurologic deficits as well as proportion of initially affected tissue progressing to infarction

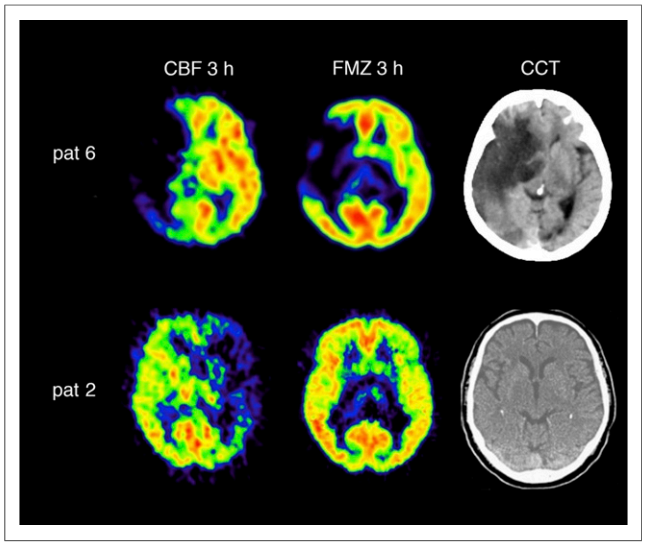

FIGURE 3. ^{11}C-flumazenil distribution and ^{11}C-flumazenil binding in patients with large ischemic areas and effect of rtPA treatment. In patient 6, with area of decreased ^{11}C-flumazenil (FMZ) binding indicating irreversible damage, rtPA was not effective and large malignant infarction developed (late cranial CT [CCT]). In patient 2, with no significant decrease of ^{11}C-flumazenil binding in area of low blood flow, reperfusion by rtPA was successful and no infarction is seen on late CT.

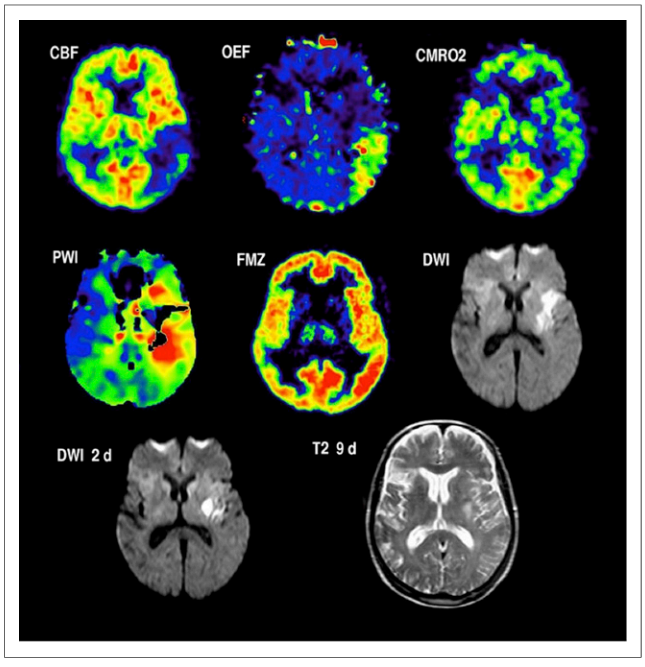

FIGURE 4. Coregistered images of multitracer PET (top row) and MR PWI and DWI (middle row) in patient with severe right-sided hemiparesis and aphasia 4 h after onset of left middle cerebral artery stroke. Penumbra is characterized by hypoperfusion (CBF), preserved $CMRO_2$, and elevated OEF (top row). These findings correspond grossly to mismatch between DWI hyperintensity in anterior and deep parts of middle cerebral artery territory and PWI delay of 4 s in posterior parts compared with unaffected hemisphere. After rtPA treatment, demarcation of small infarct on DWI on day 2 persisted on T2-weighted MR imaging (bottom row).

and neurologic deterioration during the first week after stroke are correlated. Because high ^{18}F-fluoromisonidazole uptake in these areas fulfills the definition of the penumbra, the topography of ^{18}F-fluoromisonidazole trapping was used to generate a so-called penumbragram (*61*). However, a portion of the ^{18}F-fluoromisonidazole trapping area may lie outside the final infarct and a portion of the final infarct may not exhibit early tracer uptake, indicating that ^{18}F-fluoromisonidazole trapping does not accurately identify preventable infarction and therefore may not be specific to the penumbra (*62*). The required delay between tracer injection and imaging (>2 h) further limits the value of ^{18}F-fluoromisonidazole for therapeutic decisions in acute ischemic stroke.

RADIOISOTOPE IMAGING AS A SURROGATE MARKER FOR TREATMENT EFFICIENCY AND FOR SELECTION OF PATIENTS FOR SPECIAL THERAPEUTIC STRATEGIES

The efficacy of treatment in ischemic stroke can be proven only by controlled randomized double-blind clinical trials, as successfully performed for thrombolysis with intravenous recombinant tissue plasminogen activator (rtPA) (*63*). Because such controlled trials require large patient populations collected in many stroke centers and therefore usually take a long time and considerable funds, surrogate markers are applied to predict potential therapeutic effects in small groups of patients. Effects on surrogate markers always must be confirmed in controlled trials based on sufficient patient populations. In recent years, identification of salvageable tissue by neuroimaging has gained much interest as a surrogate marker for treatment efficiency in stroke.

The effect of the only approved therapy for acute ischemic stroke was established also in imaging studies, in which reperfusion to penumbral tissue was followed by improvement in neurologic deficits (Fig. 5): reperfusion was significantly increased in rtPA-treated patients compared with controls (*64*). The volume of tissue salvaged by reperfusion was established in a study in which CBF, as determined by $H_2{}^{15}O$ PET within 3 h of stroke onset, was compared with the volume of infarction determined on MR imaging 3 wk after the ictus (*65*). The percentage of initially critically ischemic voxels (i.e., with a flow below the threshold of 12 mL/100 g/min) that became reperfused at almost normal levels clearly predicted the degree of clinical improvement achieved within 3 wk. Overall, only 22.7% of the gray matter that was initially perfused at rates below the conventional threshold of critical ischemia became necrotic after thrombolytic therapy in this small sample of 12 patients. This means that a considerable portion of the critically hypoperfused tissue was probably salvaged by the reperfusion therapy. Another PET study, on 11 patients (*66*), indicated that hypoperfused tissue could benefit from reperfusion only as long as cortical ^{11}C-flumazenil binding was not reduced to or below 3.4 times the mean uptake in white matter. This marker of neuronal integrity can therefore serve as an indicator for irreversibly damaged tissue that is not amenable to treatment.

Whereas the application of PET for the selection of patients who might benefit from treatment is rather limited, SPECT perfusion studies are easy to perform and the semiquantitative analysis of CBF in ischemic tissue is simple and prompt and can readily be implemented by any institution. CBF thresholds determined by ^{99m}Tc-HMPAO SPECT were shown to be related to the efficacy of intraarterial thrombolysis (*67*): tissue with a flow index of greater than 0.55 may still be salvageable more than 6 h after the onset of symptoms; tissue with a flow index of greater than 0.35 may still be salvageable with treatment at less than 5 h after a stroke; tissue with a flow index of below 0.35 may be at risk of hemorrhage even if treatment is started early. For intravenous rtPA therapy, pretreatment CBF values of 15%–53% obtained by ^{99m}Tc-ECD SPECT predicted irreversible lesions, whereas values of 45%–83% indicated reversible local ischemia (*68*). Posttreatment regional hypoperfusion observed by ^{99m}Tc-HMPAO SPECT was associated with a poor outcome, whereas hyperperfusion after treatment predicted symptom improvement but was not related to development of intracerebral hemorrhage (*69*).

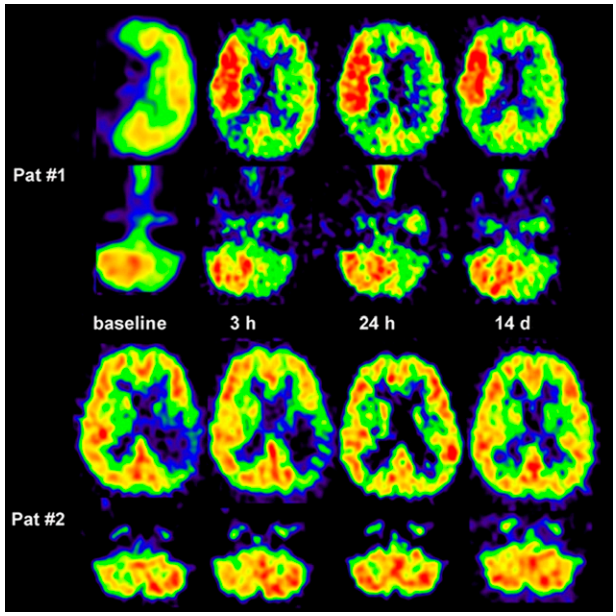

FIGURE 5. Crossed cerebellar diaschisis in acute human stroke and response to supratentorial reperfusion. In patient 1, crossed cerebellar diaschisis persisted despite marked supratentorial reperfusion or hyperperfusion. Infarct volume was 60 cm^3, and clinical outcome was poor (National Institutes of Health Stroke Scale, 9 points). In patient 2, supratentorial reperfusion was accompanied by crossed cerebellar diaschisis decrease. Follow-up CT showed no infarct; outcome score on National Institutes of Health Stroke Scale was 0 points. (Reprinted with permission of (*85*).)

Malignant brain infarcts develop in about 10% of patients with ischemic stroke in the middle cerebral artery territory. Invasive treatment strategies, especially decompressive hemicraniectomy, might improve mortality and morbidity in these patients (*70*). The selection of patients who can benefit and the determination of the best time for these interventions are, however, still controversial and require a better assessment of the extent of irreversible ischemic damage. In 34 patients with ischemic changes in more than 50% of the middle cerebral artery territory on early cerebral CT scans, PET was performed with ^{11}C-flumazenil to assess CBF and irreversible neuronal damage (Fig. 3). Afterward, probes for microdialysis and for measurement of intracranial pressure and tissue oxygen pressure were placed into the ipsilateral frontal lobe (*71*). PET measurements within 24 h after the stroke showed larger volumes of ischemic core (mean, 144.5 vs. 62.2 cm^3) and larger volumes of irreversible neuronal damage (157.9 vs. 47.0 cm^3) in patients with a malignant course (i.e., edema formation with midline shift) than in patients with a benign course (Fig. 3). Mean CBF values within the ischemic core were significantly lower and the volume of the ischemic penumbra was smaller in the malignant than in the benign group. In patients with a malignant course, cerebral perfusion pressure dropped to less than

50–60 mm Hg at 22–72 h (mean, 52.0 h) after the onset of symptoms; subsequently, tissue oxygen pressure dropped and glutamate increased, indicating secondary ischemia. Maximal changes in the monitored variables reached significant levels for glutamate, aspartate, γ-aminobutyric acid, glycerol, lactate-to-pyruvate ratio, hypoxanthine, intracranial pressure, cerebral perfusion pressure, and tissue oxygen pressure. Corresponding to the experimental results, PET allowed prediction of malignant middle cerebral artery infarction within the time window suggested for hemicraniectomy. In contrast to PET, invasive monitoring did not predict a fatal outcome early enough for successful treatment.

MICROGLIAL ACTIVATION AS AN INDICATOR OF INFLAMMATION

Microglial cells constitute up to 10% of the total cell population of the brain. They change from a resting to an activated state in response to central nervous system insults that stimulate them to function as phagocytes. As one of the consequences, the translocator protein 18 kDa, formerly known as the peripheral benzodiazepine receptor, is upregulated in mitochondria of activated microglias and may thus serve as a biomarker of inflammation. Several radioligands have been developed to image the activation of microglias in experimental models and in various diseases of the central nervous system (*72*). Applying high-resolution small-animal PET of ^{11}C-PK11195 to imaging the expression of translocator protein 18 kDa/peripheral benzodiazepine receptor in experimental ischemia, a high signal was detected in the core of ischemia starting on day 4 and increasing until day 7, and this strong signal was related to microglias and macrophages. A less prominent signal indicating elevated translocator protein 18 kDa expression was observed in the region surrounding the infarct on day 7, which was colocalized with an increased glucose metabolism and accumulated microglias and macrophages. This periinfarct neuroinflammation may contribute to the extension of tissue damage (*73*).

With PET of ^{11}C-PK11195 in humans, abundant reactive microglias and macrophages have been found in the ischemic core within 1–2 d after ischemic infarction. Over time, they extended from the ischemic core into the periinfarct zones (*74,75*). In several imaging studies, increased binding of ^{11}C-PK11195 was observed around the outer border of ischemic lesions after several days, but also in areas distant from the lesion (*72*). Increased tracer binding was also detected in the thalamus ipsilateral to the stroke and in the subcortical white matter tracts, especially along the pyramidal tract anterograde to the lesion. These portions of the tract will undergo Wallerian degeneration in the weeks and months after a stroke (*76*). The remote inflammatory activity in some instances may exert a repair function along the tract, whereas microglial activity in the area within and surrounding the infarct correlates negatively with outcome.

HEMODYNAMIC AND METABOLIC RESERVE IN ARTERIAL OCCLUSIVE DISEASE

Chronic perfusion disturbance due to arterial vascular disease is a precarious condition necessitating vascular surgery in selected cases. Vascular imaging techniques such as angiography can detect arterial occlusions or stenosis and identify collateral vessels but do not provide information on the quality of the blood supply of the tissue. Measurement of CBF alone is also inadequate for this purpose since normal CBF may be found when cerebral perfusion pressure is reduced but flow is maintained by autoregulatory vasodilation. Strategies used to determine hemodynamic and metabolic effects of arterial occlusion, especially of the carotid artery, include measurement of CBF at baseline and after application of a vasodilatory stimulus (Fig. 6), for which impairment of the resulting increase in CBF indicates reduced cerebral perfusion pressure; quantitative measurement of CBV and of CBF at rest, for which an increase in the CBV/CBF ratio indicates hemodynamic compromise; and measurement of OEF as an indicator of local autoregulating failure. On the basis of such measurements, 3 stages of hemodynamic compromise have been proposed (*45,77*): stage 0, in which collateral circulation completely compensates for the occluded artery; stage I (hemodynamic compromise), in which CBV is increased but CBF response to vasodilatory stimuli is decreased and OEF remains normal; and stage II (hemodynamic failure), in which CBF is reduced and OEF is increased to preserve $CMRO_2$ in order to cover the metabolic demands of the tissue. Abnormal OEF is a powerful predictor of subsequent ipsilateral stroke (*78*). Repeated PET scanning before and after carotid artery stenting has revealed improvements in CBF, perfusion pressure, and $CMRO_2$ (*79*), and stabilization of the hemodynamic situation has been demonstrated by SPECT (Fig. 6) (*80*) even in bilateral carotid artery disease (*81*). The exhausted metabolic reserve can lead to selective neuronal loss in the cortex, which cannot be detected by morphologic imaging with CT or MR imaging but can be documented by ^{123}I-iomazenil SPECT (*53*) or ^{11}C-flumazenil PET (*82*). However, despite selection of patients on the basis of this staging, extracranial–intracranial bypass surgery did not reduce the risk of recurrent ischemic stroke at 2 y, since the perioperative stroke rate was high and nullified any long-term benefit (*83*).

DEACTIVATION OF REMOTE TISSUE (DIASCHISIS)

Even the earliest PET studies of ischemic brain lesions (*30*) revealed reduction of metabolism and blood flow exceeding the extent of morphologically damaged tissue—a regular finding since

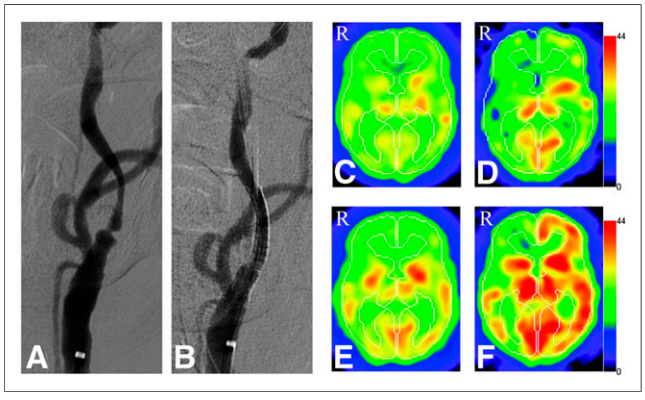

FIGURE 6. Representative case with carotid stenosis before and after stenting. (A) Preoperative left common carotid artery angiogram shows severe internal carotid artery stenosis (anteroposterior view). (B) Left carotid arterial stenting was performed, and postoperative angiogram reveals no significant residual stenosis (anteroposterior view). (C and D) Preoperative ^{123}I-isopropyl iodoamphetamine SPECT shows hypoperfusion (C) and low cerebrovascular reactivity after acetazolamide (D) in both hemispheres. In right hemisphere, steal phenomenon is detected (D). (E and F) Postoperative SPECT obtained 3 mo after carotid arterial stenting demonstrates increased resting CBF (E) and cerebrovascular reactivity (F) on both ipsilateral and contralateral carotid occluded sides. (Reprinted with permission of (*80*).)

then also with SPECT. The most conspicuous effect was a reduction of CBF and metabolism in the contralateral cerebellum, called crossed cerebellar diaschisis (*84*), occurring immediately after a stroke and persisting permanently in patients with lesions involving the corticopontocerebellar pathways but reversible by successful reperfusion therapy (Fig. 5) (*85*). This crossed cerebellar diaschisis is obviously due to some neuronally mediated effect, since the site of the acute ischemic lesion has been shown to affect the location of deactivation in the cerebellum (*86*). Further remote effects included reductions of CBF and metabolism in the ipsilateral cortex and basal ganglia. Their cause was less clear since selective ischemic neuronal loss or inadequate blood supply could also contribute in these areas. However, because similar effects have also been observed in nonischemic lesions such as brain tumors and intracerebral hematomas, these effects therefore seem to be more closely related to the site than to the nature of the primary lesion (*84*). Among cortical and subcortical lesions, infarcts of the parietal and frontal lobes most often cause significant reductions of CBF and metabolism in the ipsilateral basal ganglia and the contralateral cerebellum. This observation might be explained by damage to corticopontocerebellar pathways. Infarcts of the basal ganglia may cause ipsilateral cerebral as well as contralateral cerebellar deactivation. Thalamic infarcts have mainly diffuse ipsilateral cortical effects, and significant cerebellar deactivations appear only when the internal capsule is involved in the lesion (*87*). Infarcts of the brain stem and the cerebellum usually do not cause significant asymmetric inactivations of forebrain structures. Diaschisis cannot reliably be detected by the usual PWI parameters. Clinical symptoms that are difficult to relate to the infarct proper can often be explained by remote effects, and the degree of diaschisis appears to be related to the severity of clinical deficits (assessed by stroke scales) and to later functional recovery (*88*). Deactivation and reactivation in specialized parts of a functional network may play a major role for the presentation of clinical syndromes and their recovery.

ACTIVATION STUDIES IN STROKE PATIENTS

Infarcted tissue cannot be replaced or regenerated in the adult human brain; therefore, improvement or recovery of neurologic deficits can be achieved only by reactivation of functionally disturbed but morphologically preserved areas or by recruitment of alternative pathways within the functional network. These compensatory mechanisms are expressed in altered patterns of blood flow or metabolism at rest and during activation within the network involved in a task and can be studied by radioisotope methods as already reported with the xenon technique (*89*) and with early PET applications (*90*). Neuroimaging studies include measurements at rest, comparing location and extent to deficit and outcome, and measurements during activation tasks, comparing changes in activation patterns to functional performance. Longitudinal assessments at rest and during activation tasks during the early and later periods after a stroke can demonstrate recruitment and compensatory mechanisms in the functional network responsible for complete or partial recovery of disturbed functions (*91*).

The degree of motor impairment and the potential for motor recovery depend on the site of the lesion, the combination of lesions in cortical areas and fiber tracts, and the involvement of gray structures in the depth of the brain, such as the basal ganglia, thalamus, and brain stem. The patterns of altered metabolism and blood flow and the patterns of activation after stimuli or during motor tasks are manifold and reflect the site and extent of the lesion, but they are also dependent on the paradigm of stimulus or task.

In most PET studies involving active or passive movements, widespread networks were activated in both hemispheres. Although changes in both the damaged and the undamaged hemisphere can be observed, ipsilateral activation of the motor cortex is consistently found to be stronger for movement of the paretic fingers after recovery from stroke. In contrast, movements of the unaffected hand (as in healthy subjects) are accompanied mainly by activation of the contralateral cerebral cortex. In addition to stronger intensity, the spatial extent of activation in the motor cortex is enlarged, and activation on the ipsilateral side is also seen in the premotor and insular cortex. Task-oriented arm training increased activation bilaterally in the inferior parietal area, in premotor areas, and in the contralateral sensorimotor cortex, suggesting bilateral functional brain reorganization (*92*). Newly learned movements after focal cortical injury are represented over larger cortical territories, an effect that appears to be dependent on the intensity of rehabilitative training. It has also been shown that the unaffected hemisphere actually inhibits the generation of a voluntary movement by the paretic hand (*93*), and this effect of transcallosal inhibition can be reduced by repetitive transcranial magnetic stimulation (*94*). Recovery from infarction is also accompanied by substantial changes in the activity of the proprioceptive systems of the paretic and nonparetic limbs, reflecting an interhemispheric shift of attention to proprioceptive stimuli associated with recovery.

Regarding poststroke aphasia, in right-handed individuals with language dominance in the left hemisphere, the left temporoparietal region is most frequently impaired, and the degree of impairment is related to the severity of the aphasia. The functional disturbance as measured by rCMRGlc in speech-relevant brain regions early after stroke has been shown to be predictive of the eventual outcome of aphasia; moreover, the metabolism in the hemisphere outside the infarct was also significantly related to the outcome of poststroke aphasia (*95*). The functionality of the bihemispheric network has a significant impact on outcome: although the brain recruits right-hemispheric regions for speech processing when the left-hemispheric centers are impaired, outcome studies have revealed that this strategy is significantly less effective than repair of the speech-relevant network in adults (Fig. 7) (*96*).

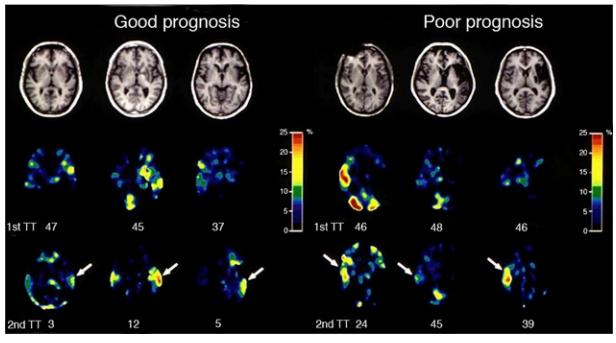

FIGURE 7. T1-weighted transaxial MR images (top row) and images of relative metabolic increase in PET (middle and bottom rows) in 6 patients with poststroke aphasia. Middle row shows metabolic increase during single-word repetition in subacute state after stroke, and bottom row shows metabolic increase more than 1 y after stroke. Numbers below images of metabolic increase give number of token test (TT) errors at time of PET. The 3 patients on the right had poor outcome of aphasia and showed maximum metabolic activation of right superior temporal cortex, whereas the 3 patients on the left, with better outcome, showed recovery of metabolic activation in left superior temporal cortex (arrows).

Patients with subcortical and frontal lesions improved substantially and regained regional left supramarginal temporal gyrus activation at follow-up. Patients with temporal lesions improved only in word comprehension and could not reactivate the left supramarginal temporal gyrus. Aphasia recovery after stroke was improved by the use of inhibitory repetitive magnetic stimulation on the right inferior frontal gyrus, which favored recruitment of left-hemispheric language networks: the shift of activation observed in PET correlated to improved performance on aphasia tests (*97*).

CONCLUSION AND FUTURE PERSPECTIVES

Because of the complex logistics involved with radionuclide imaging, especially for the quantification of physiologic and molecular variables, its role in the clinical management of stroke and occlusive cerebrovascular disease is limited. For clinical management of acute cerebrovascular disease, direct and easy access to imaging is required, as is obtainable by MR imaging and CT, and these imaging modalities are the workhorses in stroke care. However, molecular imaging, especially PET, had and still has a major input in research of the pathophysiology of ischemic damage and for the development of new treatment strategies and should additionally be used to validate indicators of pathophysiologic changes obtained by noninvasive procedures.

Multimodal imaging of physiologic and metabolic variables by PET requires coregistration to CT or MR imaging for accurate correspondence to the anatomic structures and to pathologic changes. MR is the best method to image the morphology of the brain in health and disease, and various MR modalities can additionally be used to assess physiologic and metabolic parameters such as vascular supply (contrast-enhanced MR imaging), perfusion (PWI), edema (DWI), functional activation (functional MR imaging), and concentration of defined substrates (MR spectroscopy). The combination of both technologies in hybrid systems is already being applied in experimental research to assess simultaneously metabolism in the picomolar range from PET and in the micromolar range from high-resolution MR imaging and has promising potential in humans (*98*).

A hybrid system guarantees the same physiologic state for comparative measurements of perfusion by PET and MR imaging. It permits differentiation of the core from the penumbra and can be used to validate a PWI–DWI mismatch. It demonstrates time-dependent growth of infarction and may be used to determine the optimal therapy for a certain time after the stroke. The vascular origin of the stroke can be detected by MRA, and perfusion or oxyhemoglobin and deoxyhemoglobin changes (blood oxygenation level–dependent effect) can be related to the extent of oxygen deprivation (^{15}O) and hypoxia (^{18}F-fluoromisonidazole) and to changes in metabolic markers (^{18}F-FDG PET, MR spectroscopy for lactate, choline, *N*-acetylaspartate)—complementary information important for therapeutic decisions. This high-resolution anatomic information is complemented by diffusion-based tractography and can be related to activation or inhibition of neurotransmitter and neuroreceptor activity as well as to inflammatory reactions. By combining MR spectroscopy and PET, one can detect other molecules important in glucose metabolism, such as lactate and pyruvate, and determine nonoxidative glycolysis in acute ischemia.

Some innovative strategies might result from the transfer of experimental findings into clinical applications of PET/MR: imaging of angiogenesis by ^{18}F-galacto-RGD (a cyclic growth factor receptor peptide) combined with dynamic contrast-enhanced MR may become feasible and yields information on revascularization processes in the course after stroke (*99*). Monitoring the location and following the migration of grafted stem or progenitor cells will be essential in the development of cell replacement strategies for treatment of various neurologic disorders. These cells can be labeled with iron oxide particles, and their survival and migration to the ischemic lesion can be followed by MR imaging (*100*). A combination of MR imaging for tracking cells and of PET for proving their biologic activity may demonstrate the viability of the cells as well as their integration into functional networks. With these perspectives, imaging with radioisotopes still has a promising future for research in cerebral ischemia and for clinical management of stroke patients.

REFERENCES

1. Kety SS, Schmidt CF. The determination of cerebral blood flow in man by the use of nitrous oxide in low concentrations. *Am J Physiol.* 1945;143:53–66.
2. Ingvar DH, Lassen NA. Quantitative determination of regional cerebral blood flow in man. *Lancet.* 1961;278:806–807.
3. Glass HI, Harper AM. Measurement of regional blood flow in cerebral cortex of man through intact skull. *Br Med J.* 1963;1:593.
4. Ingvar DH, Cronqvist S, Ekberg R, Risberg J, Hoedt-Rasmussen K. Normal values of regional cerebral blood flow in man, including flow and weight estimates of grey and white matter. *Acta Neurol Scand.* 1965;41(suppl 14):72–78.
5. Heiss WD, Prosenz P, Roszuczky A. Technical considerations in the use of a gamma camera 1,600-channel analyzer system for the measurement of regional cerebral blood flow. *J Nucl Med.* 1972;13:534–543.
6. Hoedt-Rasmussen K, Skinhoj E, Paulson O, et al. Regional cerebral blood flow in acute apoplexy: the "luxury perfusion syndrome" of brain tissue. *Arch Neurol.* 1967;271–281.
7. Kuhl DE, Edwards RQ, Ricci AR, Yacob RJ, Mich TJ, Alavi A. The Mark IV system for radionuclide computed tomography of the brain. *Radiology.* 1976;121:405–413.
8. Ter-Pogossian MM, Phelps ME, Hoffman EJ, Mullani NA. A positron emission transaxial tomograph for nuclear imaging (PETT). *Radiology.* 1975;114:89–98.
9. Pakkenberg B, Gundersen HJ. Neocortical neuron number in humans: effect of sex and age. *J Comp Neurol.* 1997;384:312–320.
10. Clarke DD, Sokoloff L. Circulation and energy metabolism of the brain. In: Siegel G, Agranoff B, Albers RW, Fisher S, eds. *Basic Neurochemistry: Molecular, Cellular, and Medical Aspects*. 6th ed. Philadelphia, PA: Lippincott-Raven; 1999:637–669.
11. Howarth C, Gleeson P, Attwell D. Updated energy budgets for neural computation in the neocortex and cerebellum. *J Cereb Blood Flow Metab.* 2012;32:1222–1232.
12. Reivich M, Kuhl D, Wolf A, et al. The [^{18}F]fluorodeoxyglucose method for the measurement of local cerebral glucose utilization in man. *Circ Res.* 1979;44:127–137.
13. Silverman DHS, Melega WP. Molecular imaging of biologic processes with PET: evaluating biologic bases of cerebral function. In: Phelps ME, ed. *PET: Molecular Imaging and Its Biological Application*. New York, NY: Springer; 2003:509–583.
14. Holman BL, Devous MD Sr. Functional brain SPECT: the emergence of a powerful clinical method. *J Nucl Med.* 1992;33:1888–1904.
15. Asenbaum S, Brücke T, Pirker W, Pietrzyk U, Podreka I. Imaging of cerebral blood flow with technetium-99m-HMPAO and technetium-99m-ECD: a comparison. *J Nucl Med.* 1998;39:613–618.
16. Matsuda H, Yagishita A, Tsuji S, Hisada K. A quantitative approach to technetium-99m ethyl cysteinate dimer: a comparison with technetium-99m hexamethylpropylene amine oxime. *Eur J Nucl Med.* 1995;22:633–637.
17. Lassen NA, Henriksen L, Paulson OB. Regional cerebral blood flow by radioxenon-113 inhalation and dynamic emission tomography. *Prog Nucl Med.* 1981;7:110–117.
18. Phelps ME, Huang SC, Hoffman EJ, Kuhl DE. Validation of tomographic measurement of cerebral blood volume with C-11-labeled carboxyhemoglobin. *J Nucl Med.* 1979;20:328–334.
19. Martin WRW, Powers WJ, Raichle ME. Cerebral blood volume measured with inhaled C^{15}O and positron emission tomography. *J Cereb Blood Flow Metab.* 1987;7:421–426.
20. Raichle ME, Martin WR, Herscovitch P, Mintun MA, Markham J. Brain blood flow measured with intravenous $H_2{}^{15}O$. II. Implementation and validation. *J Nucl Med.* 1983;24:790–798.

21. Frackowiak RSJ, Lenzi GL, Jones T, Heather JD. Quantitative measurement of regional cerebral blood flow and oxygen metabolism in man using ^{15}O and positron emission tomography: theory, procedure, and normal values. *J Comput Assist Tomogr.* 1980;4:727–736.
22. Mintun MA, Raichle ME, Martin WRW, Herscovitch P. Brain oxygen utilization measured with O-15 radiotracers and positron emission tomography. *J Nucl Med.* 1984;25:177–187.
23. Huang SC, Feng DG, Phelps ME. Model dependency and estimation reliability in measurement of cerebral oxygen utilization rate with oxygen-15 and dynamic positron emission tomography. *J Cereb Blood Flow Metab.* 1986;6:105–119.
24. Sokoloff L, Reivich M, Kennedy C, et al. The [^{14}C]deoxyglucose method for the measurement of local cerebral glucose utilization: theory, procedure, and normal values in the conscious and anesthetized albino rat. *J Neurochem.* 1977;28:897–916.
25. Paulson OB. Cerebral apoplexy (stroke): pathogenesis, pathophysiology and therapy as illustrated by regional blood flow measurements in the brain. *Stroke.* 1971;2:327–360.
26. Heiss WD. Regional cerebral blood flow measurement using a scintillation camera. *Clin Nucl Med.* 1979;4:385–396.
27. Kushner M, Reivich M, Fieschi C, et al. Metabolic and clinical correlates of acute ischemic infarction. *Neurology.* 1987;37:1103–1110.
28. Raynaud C, Rancurel G, Tzourio N, et al. SPECT analysis of recent cerebral infarction. *Stroke.* 1989;20:192–204.
29. Brass LM, Walovitch RC, Joseph JL, et al. The role of single photon emission computed tomography brain imaging with ^{99m}Tc-bicisate in the localization and definition of mechanism of ischemic stroke. *J Cereb Blood Flow Metab.* 1994; 14(suppl 1):S91–S98.
30. Kuhl DE, Phelps ME, Kowell AP, Metter EJ, Selin C, Winter J. Effects of stroke on local cerebral metabolism and perfusion: mapping by emission computed tomography of ^{18}FDG and $^{13}NH_3$. *Ann Neurol.* 1980;8:47–60.
31. Wise RJS, Bernardi S, Frackowiak RSJ, Legg NJ, Jones T. Serial observations on the pathophysiology of acute stroke: the transition from ischaemia to infarction as reflected in regional oxygen extraction. *Brain.* 1983;106:197–222.
32. Lassen NA. The luxury-perfusion syndrome and its possible relation to acute metabolic acidosis localized within the brain. *Lancet.* 1966;2:1113–1115.
33. Berrouschot J, Barthel H, Hesse S, Koster J, Knapp WH, Schneider D. Differentiation between transient ischemic attack and ischemic stroke within the first 6 hours after onset of symptoms by using ^{99m}Tc-ECD-SPECT. *J Cereb Blood Flow Metab.* 1998;18:921–929.
34. Powers WJ. Cerebral hemodynamics in ischemic cerebrovascular disease. *Ann Neurol.* 1991;29:231–240.
35. Ueda T. Can the penumbra be imaged using single-photon emission computed tomography? In: Donnan GA, Baron JC, Davis SM, Sharp FR, eds. *The Ischemic Penumbra*. Boca Raton, FL: CRC Press; 2007:165–175.
36. Marchal G, Serrati C, Rioux P, et al. PET imaging of cerebral perfusion and oxygen consumption in acute ischaemic stroke: relation to outcome. *Lancet.* 1993;341:925–927.
37. Hossmann KA. Pathophysiological basis of translational stroke research. *Folia Neuropathol.* 2009;47:213–227.
38. Astrup J, Siesjö BK, Symon L. Thresholds in cerebral ischemia: the ischemic penumbra. *Stroke.* 1981;12:723–725.
39. Heiss WD, Rosner G. Functional recovery of cortical neurons as related to degree and duration of ischemia. *Ann Neurol.* 1983;14:294–301.
40. Ackerman RH, Correia JA, Alpert NM, et al. Positron imaging in ischemic stroke disease using compounds labeled with oxygen 15: initial results of clinicophysiologic correlations. *Arch Neurol.* 1981;38:537–543.
41. Baron JC, Bousser MG, Comar D, Soussaline F, Castaigne P. Noninvasive tomographic study of cerebral blood flow and oxygen metabolism in vivo: potentials, limitations, and clinical applications in cerebral ischemic disorders. *Eur Neurol.* 1981;20:273–284.
42. Lenzi GL, Frackowiak RSJ, Jones T. Cerebral oxygen metabolism and blood flow in human cerebral ischemic infarction. *J Cereb Blood Flow Metab.* 1982;2:321–335.
43. Powers WJ, Grubb RL Jr, Darriet D, Raichle ME. Cerebral blood flow and cerebral metabolic rate of oxygen requirements for cerebral function and viability in humans. *J Cereb Blood Flow Metab.* 1985;5:600–608.
44. Heiss WD. Ischemic penumbra: evidence from functional imaging in man. *J Cereb Blood Flow Metab.* 2000;20:1276–1293.
45. Powers WJ, Zazulia AR. PET in cerebrovascular disease. *PET Clin.* 2010;5: 83106.
46. Baron JC. Mapping the ischaemic penumbra with PET: implications for acute stroke treatment. *Cerebrovasc Dis.* 1999;9:193–201.
47. Heiss WD, Huber M, Fink GR, et al. Progressive derangement of periinfarct viable tissue in ischemic stroke. *J Cereb Blood Flow Metab.* 1992;12:193–203.
48. Sasaki O, Takeuchi S, Koizumi T, Koike T, Tanaka R. Complete recanalization via fibrinolytic therapy can reduce the number of ischemic territories that progress to infarction. *Am J Neuroradiol.* 1996;17:1661–1668.
49. Iseda T, Nakano S, Yano T, Suzuki Y, Wakisaka S. Time-threshold curve determined by single photon emission CT in patients with acute middle cerebral artery occlusion. *AJNR.* 2002;23:572–576.
50. Watanabe Y, Takagi H, Aoki S, Sassa H. Prediction of cerebral infarct sizes by cerebral blood flow SPECT performed in the early acute stage. *Ann Nucl Med.* 1999;13:205–210.
51. Umemura A, Suzuka T, Yamada K. Quantitative measurement of cerebral blood flow by ^{99m}Tc-HMPAO SPECT in acute ischaemic stroke: usefulness in determining therapeutic options. *J Neurol Neurosurg Psychiatry.* 2000;69:472–478.
52. Guadagno JV, Jones PS, Aigbirhio FI, et al. Selective neuronal loss in rescued penumbra relates to initial hypoperfusion. *Brain.* 2008;131:2666–2678.
53. Nakagawara J, Sperling B, Lassen NA. Incomplete brain infarction of reperfused cortex may be quantitated with iomazenil. *Stroke.* 1997;28:124–132.
54. Chida K, Ogasawara K, Kuroda H, et al. Central benzodiazepine receptor binding potential and CBF images on SPECT correlate with oxygen extraction fraction images on PET in the cerebral cortex with unilateral major cerebral artery occlusive disease. *J Nucl Med.* 2011;52:511–518.
55. Saur D, Buchert R, Knab R, Weiller C, Rother J. Iomazenil-single-photon emission computed tomography reveals selective neuronal loss in magnetic resonance-defined mismatch areas. *Stroke.* 2006;37:2713–2719.
56. Kidwell CS, Alger JR, Saver JL. Beyond mismatch: evolving paradigms in imaging the ischemic penumbra with multimodal magnetic resonance imaging. *Stroke.* 2003;34:2729–2735.
57. Sobesky J, Weber OZ, Lehnhardt FG, et al. Does the mismatch match the penumbra? Magnetic resonance imaging and positron emission tomography in early ischemic stroke. *Stroke.* 2005;36:980–985.
58. Zaro-Weber O, Moeller-Hartmann W, Heiss W-D, Sobesky J. The performance of MRI-based cerebral blood flow measurements in acute and subacute stroke compared with ^{15}O-water positron emission tomography: identification of penumbral flow. *Stroke.* 2009;40:2413–2421.
59. Yeh SH, Liu RS, Hu HH, et al. Ischemic penumbra in acute stroke: demonstration by PET with fluorine-18 fluoromisonidazole [abstract]. *J Nucl Med.* 1994; 35(suppl):205P.
60. Read SJ, Hirano T, Abbott DF, et al. Identifying hypoxic tissue after acute ischemic stroke using PET and ^{18}F-fluoromisonidazole. *Neurology.* 1998;51:1617–1621.
61. Markus R, Donnan G, Kazui S, Read S, Reutens D. Penumbral topography in human stroke: methodology and validation of the 'Penumbragram.' *Neuroimage.* 2004;21:1252–1259.
62. Alawneh JA, Moustafa RR, Marrapu ST, et al. Diffusion and perfusion correlates of the ^{18}F-MISO PET lesion in acute stroke: pilot study. *Eur J Nucl Med Mol Imaging.* 2014;41:736–744.
63. Lees KR, Bluhmki E, von Kummer R, et al. Time to treatment with intravenous alteplase and outcome in stroke: an updated pooled analysis of ECASS, ATLANTIS, NINDS, and EPITHET trials. *Lancet.* 2010;375:1695–1703.
64. Grotta JC, Alexandrov AV. tPA-associated reperfusion after acute stroke demonstrated by SPECT. *Stroke.* 1998;29:429–432.
65. Heiss WD, Grond M, Thiel A, et al. Tissue at risk of infarction rescued by early reperfusion: a positron emission tomography study in systemic recombinant tissue plasminogen activator thrombolysis of acute stroke. *J Cereb Blood Flow Metab.* 1998;18:1298–1307.
66. Heiss WD, Kracht L, Grond M, et al. Early [^{11}C]flumazenil/H_2O positron emission tomography predicts irreversible ischemic cortical damage in stroke patients receiving acute thrombolytic therapy. *Stroke.* 2000;31:366–369.
67. Ueda T, Sakaki S, Yuh WTC, Nochide I, Ohta S. Outcome in acute stroke with successful intra-arterial thrombolysis and predictive value of initial single-photon emission-computed tomography. *J Cereb Blood Flow Metab.* 1999;19:99–108.
68. Nakano S, Iseda T, Ikeda T, Yoneyama T, Wakisaka S. Thresholds of ischemia salvageable with intravenous tissue plasminogen activator therapy: evaluation with cerebral blood flow single-photon emission computed tomographic measurements. *Neurosurgery.* 2000;47:68–71.
69. Abumiya T, Katoh M, Moriwaki T, et al. Utility of early post-treatment single-photon emission computed tomography imaging to predict outcome in stroke patients treated with intravenous tissue plasminogen activator. *J Stroke Cerebrovasc Dis.* 2014;23:896–901.
70. Jüttler E, Bosel J, Amiri H, et al. DESTINY II: DEcompressive Surgery for the Treatment of malignant INfarction of the middle cerebral arterY II. *Int J Stroke.* 2011;6:79–86.
71. Dohmen C, Bosche B, Graf R, et al. Prediction of malignant course in middle cerebral artery infarction by PET and microdialysis. *Stroke.* 2003;34:2152–2158.
72. Thiel A, Heiss WD. Imaging of microglia activation in stroke. *Stroke.* 2011;42: 507–512.

73. Schroeter M, Dennin MA, Walberer M, et al. Neuroinflammation extends brain tissue at risk to vital peri-infarct tissue: a double tracer [^{11}C]PK11195- and [^{18}F]FDG-PET study. *J Cereb Blood Flow Metab.* 2009;29:1216–1225.
74. Weinstein JR, Koerner IP, Moller T. Microglia in ischemic brain injury. *Future Neurol.* 2010;5:227–246.
75. Gerhard A, Schwarz J, Myers R, Wise R, Banati RB. Evolution of microglial activation in patients after ischemic stroke: a [^{11}C](R)-PK11195 PET study. *Neuroimage.* 2005;24:591–595.
76. Radlinska BA, Ghinani SA, Lyon P, et al. Multimodal microglia imaging of fiber tracts in acute subcortical stroke. *Ann Neurol.* 2009;66:825–832.
77. Gibbs JM, Wise RJ, Leenders KL, Jones T. Evaluation of cerebral perfusion reserve in patients with carotid-artery occlusion. *Lancet.* 1984;1:310–314.
78. Gupta A, Baradaran H, Schweitzer AD, et al. Oxygen extraction fraction and stroke risk in patients with carotid stenosis or occlusion: a systematic review and meta-analysis. *AJNR.* 2014;35:250–255.
79. Matsubara S, Moroi J, Suzuki A, et al. Analysis of cerebral perfusion and metabolism assessed with positron emission tomography before and after carotid artery stenting: clinical article. *J Neurosurg.* 2009;111:28–36.
80. Oka F, Ishihara H, Kato S, Higashi M, Suzuki M. Cerebral hemodynamic benefits after contralateral carotid artery stenting in patients with internal carotid artery occlusion. *AJNR.* 2013;34:616–621.
81. Abe A, Ueda T, Ueda M, Nogoshi S, Nishiyama Y, Katayama Y. Recovery of cerebrovascular reserves after stenting for symptomatic carotid artery stenosis. *Interv Neuroradiol.* 2010;16:420–428.
82. Baron JC, Yamauchi H, Fujioka M, Endres M. Selective neuronal loss in ischemic stroke and cerebrovascular disease. *J Cereb Blood Flow Metab.* 2014;34:2–18.
83. Powers WJ, Clarke WR, Grubb RL Jr, et al. Extracranial-intracranial bypass surgery for stroke prevention in hemodynamic cerebral ischemia: the Carotid Occlusion Surgery Study randomized trial. *JAMA.* 2011;306:1983–1992.
84. Feeney DM, Baron JC. Diaschisis. *Stroke.* 1986;17:817–830.
85. Sobesky J, Thiel A, Ghaemi M, et al. Crossed cerebellar diaschisis in acute human stroke: a PET study of serial changes and response to supratentorial reperfusion. *J Cereb Blood Flow Metab.* 2005;25:1685–1691.
86. Liu Y, Karonen JO, Nuutinen J, Vanninen E, Kuikka JT, Vanninen RL. Crossed cerebellar diaschisis in acute ischemic stroke: a study with serial SPECT and MRI. *J Cereb Blood Flow Metab.* 2007;27:1724–1732.
87. Szelies B, Herholz K, Pawlik G, Karbe H, Hebold I, Heiss WD. Widespread functional effects of discrete thalamic infarction. *Arch Neurol.* 1991;48:178–182.
88. Szilágyi G, Vas A, Kerenyi L, Nagy Z, Csiba L, Gulyas B. Correlation between crossed cerebellar diaschisis and clinical neurological scales. *Acta Neurol Scand.* 2012;125:373–381.
89. Ingvar DH. Functional landscapes of the dominant hemisphere. *Brain Res.* 1976;107:181–197.
90. Phelps ME, Mazziotta JC. Positron emission tomography: human brain function and biochemistry. *Science.* 1985;228:799–809.
91. Rijntjes M, Weiller C. Recovery of motor and language abilities after stroke: the contribution of functional imaging. *Prog Neurobiol.* 2002;66:109–122.
92. Nelles G, Jentzen W, Jueptner M. Müller S, Diener HC. Arm training induced brain plasticity in stroke studied with serial positron emission tomography. *Neuroimage.* 2001;13:1146–1154.
93. Murase N, Duque J, Mazzocchio R, Cohen LG. Influence of interhemispheric interactions on motor function in chronic stroke. *Ann Neurol.* 2004;55:400–409.
94. Hsu WY, Cheng CH, Liao KK, Lee IH, Lin YY. Effects of repetitive transcranial magnetic stimulation on motor functions in patients with stroke: a meta-analysis. *Stroke.* 2012;43:1849–1857.
95. Heiss WD, Thiel A, Winhuisen L, Mühlberger B, Kessler J, Herholz K. Functional imaging in the assessment of capability for recovery after stroke. *J Rehabil Med.* 2003;41:27–33.
96. Saur D, Lange R, Baumgaertner A, et al. Dynamics of language reorganization after stroke. *Brain.* 2006;129:1371–1384.
97. Thiel A, Hartmann A, Rubi-Fessen I, et al. Effects of noninvasive brain stimulation on language networks and recovery in early poststroke aphasia. *Stroke.* 2013;44:2240–2246.
98. Catana C, Drzezga A, Heiss WD, Rosen BR. PET/MRI for neurologic applications. *J Nucl Med.* 2012;53:1916–1925.
99. Hsu AR, Chen X. Advances in anatomic, functional, and molecular imaging of angiogenesis. *J Nucl Med.* 2008;49:511–514.
100. Hoehn M, Himmelreich U, Kruttwig K, Wiedermann D. Molecular and cellular MR imaging: potentials and challenges for neurological applications. *J Magn Reson Imaging.* 2008;27:941–954.

The Journal of NUCLEAR MEDICINE

Radionuclide Imaging in Ischemic Stroke

Wolf-Dieter Heiss

J Nucl Med. 2014;55:1831-1841.
Published online: October 9, 2014.
Doi: 10.2967/jnumed.114.145003

The Journal of Nuclear Medicine is published monthly.
SNMMI | Society of Nuclear Medicine and Molecular Imaging
1850 Samuel Morse Drive, Reston, VA 20190.
(Print ISSN: 0161-5505, Online ISSN: 2159-662X)

SNMMI SOCIETY OF NUCLEAR MEDICINE AND MOLECULAR IMAGING